Heliyon 9 (2023) e21417

Contents lists available at ScienceDirect

Heliyon

journal homepage: www.cell.com/heliyon

The effects of formation and functionalization of graphene-based membranes on their gas and water vapor permeation properties

Darina Smržová [a], Michaela Šrámová Slušná [a], Jakub Peter [b], Hynek Beneš [b], Jakub Tolasz [a], Ognen Pop Georgievski [b], Monika Maříková [a], Petra Ecorchard [a,*]

[a] Institute of Inorganic Chemistry of the Czech Academy of Sciences, 250 68 Husinec- Řež, Czech Republic
[b] Institute of Macromolecular Chemistry of the Czech Academy of Sciences, Heyrovského nám. 2, 162 06 Prague 6, Czech Republic

ARTICLE INFO

Keywords:
Graphene oxide
Carboxylated graphene oxide
Graphene-based membrane
Gas permeability

ABSTRACT

The gas and water vapor permeabilities of graphene-based membranes can be affected by the presence of different functional groups directly bound to the graphene network. In this work, one type of carboxylated graphene oxide (GO-COOH) and two types of graphene oxide synthesized i) under strong oxidative conditions directly from graphite (GO-1) and ii) under mild oxidative conditions from exfoliated graphene (GO-2) were used as precursors of self-standing membranes prepared with thicknesses in the range of 12–55 μm via slow-vacuum filtration preparation method. It was observed that the permeabilities for all tested gases decreased in order GO-2 > GO-1 > GO-COOH and depended on both the arrangement of graphene sheets and their functionalization. The GO-1 membrane with a high content of oxygen-containing groups showed the best performance for water vapor permeability. The GO-2 membrane with a thickness of 43 μm exhibited a disordered GO sheet morphology and, therefore, unique gas-separation performance towards H_2/CO_2 gas pair, showing high hydrogen permeability while keeping extremely high H_2/CO_2 ideal selectivity that exceeds the Robeson 2008 upper bound of polymer membranes.

1. Introduction

Membranes with suitable properties (good permeabilities, thickness, etc.) are important for gas separation and other separation processes, e.g., water purification or wastewater treatment [1–3]. Membranes from materials such as polymers and zeolites are applied in industry. However, their use is limited due to permeability and selectivity reasons (mesoporous material has limitations concerning gas separation) [4,5]. Recently, attention has been shifted to carbon-based nanomaterials such as carbon nanotubes, graphene and graphene oxide (GO) for their excellent mechanical properties, high chemical resistance [6–9], tuneable ionic selectivity [10–12], low manufacturing costs [11,13], biocompatibility, and environmental friendliness [5]. Gkika et al. [14] recently reviewed progress in membranes coated with graphene materials with respect to design, production and use. Ahmad et al. [15] published a review concentrated on graphene-based membranes specifically for hydrogen separation. High permeability is the advantage of carbon nanotube and graphene membranes, but they are difficult to manipulate, while the opposite is valid for GO membranes [16]. GO involves oxygen-containing (carboxyl, hydroxyl and epoxy) functional groups. Due to its hydrophilic character, GO can be well dispersed in aqueous solutions. GO layers can be arranged by vacuum filtrations, spin coating or other methods [17]. Romanos et al.

* Corresponding author
E-mail address: ecorchard@iic.cas.cz (P. Ecorchard).

https://doi.org/10.1016/j.heliyon.2023.e21417
Received 14 June 2023; Received in revised form 12 October 2023; Accepted 20 October 2023
Available online 21 October 2023

prepared GO membranes with a thickness of 7–20 μm and demonstrated that GO porosity strongly depends on the filtration rate: fast filtration produced GO membranes with high porosity, while very slow filtration led to low-porous membranes. Moreover, the membranes with a lower concentration of oxygen surface groups showed high water vapor performances, which could be advantageous for membrane distillation processes [18]. Achari et al. [19] enhanced GO permeability by annealing at 80 °C while retaining selectivity. The creation of oxygen-rich and graphitic regions formed channels. A high H_2/CO_2 separation factor of up to 240 was achieved. Outstanding H_2/CO_2 separation by using GO membranes is also reported by Chi et al. [20], Bouša et al. [21] and Shen et al. [22]. According to Bouša et al. [21], specific hydrogen bonding interactions of permeating molecules with carboxyl and hydroxyl functional GO groups and quadruple moment contributed to CO_2 gas transport. Ibrahim et al. [23] prepared GO membranes by spray coating to avoid wrinkles occurring during the most common preparation method by filtration and also utilize the scaling possibility. Lately, tailoring defects of GO have been investigated. Wei et al. [24] prepared GO films (thickness ~150 nm) and modified them with a low-energy carbon beam that resulted in the simultaneous reduction and drilling of nanoscale pores. Huang et al. [25] modified GO (before membrane fabrication) by hydrogen peroxide etching to generate in-plane nanopores.

Modifications of GO membranes have been mainly investigated for ion separations in water environments [26]. Chemical modifications of GO for gas separation purposes have scarcely appeared in the literature. Crosslinking and intercalation of La^{3+} or Co^{2+} cations between GO layers enabled tuning of interlayer spacing [27]. The increased d-spacing together with restricted defect formation resulted in high H_2/CO_2 selectivity of the GO-La^{3+} laminate membrane. Wu et al. [28] demonstrated computationally the excellent properties of fluorine-modified porous graphene membranes for CO_2/N_2 separation. Based on the findings mentioned above, it seems that the gas permeation of graphene-based membranes can be highly affected by preparation methods and membrane composition.

In this work, we studied the effect of graphene-derived precursors with different amounts and distribution of functional (oxygen-containing) groups on the preparation and permeation properties of graphene-based membranes. In the first step, three types of graphene-derived precursors were synthesized; two types of GO, denoted GO-1 and GO-2 synthesized via the classic Hummers' method [29] and the method previously published by our group [30,31], respectively, and one type of carboxylated GO (GO-COOH) [32,33]. The content of functional groups was determined for the precursors, as they enable interactions with molecules of penetrating gases and water vapor. In the next step, these precursors were used to prepare graphene-based membranes by vacuum filtration. The membrane preparation method was optimized to obtain the thinnest possible but self-standing and defect-free membrane-enabling permeation experiments. The morphology of the formed membranes was another important piece of information to better understand the separation system's mechanism. Moreover, the effect of variable membrane thickness on the permeability, diffusion and sorption of CO_2, H_2, N_2 and water vapor was also determined.

2. Experimental

2.1. Chemicals

All chemicals for GO-COOH and GO preparations were supplied by Lach-ner Ltd. (Neratovice, Czech Republic), chloroacetic acid, 85 % H3PO4, 96 % H_2SO_4, $KMnO_4$, and H2O2. The solvent (ethylene glycol) was purchased from Penta Ltd., and synthetic graphite was supplied by Graphite Týn Ltd. (Týn nad Vltavou, Czech Republic).

2.2. Preparation of graphene-derived precursors

2.2.1. Graphene oxide (GO-1 and GO-2)

Two types of GO were prepared under different reaction conditions using synthetic protocols already described before [29–31]. The first synthetic route producing GO-1 is a modified Hummers' method [29] and uses a much higher concentration of oxidation agents (graphite oxidation with $KMnO_4$ in a 9:1 mixture of concentrated H_2SO_4/H_3PO_4 acids) than the second method leading to GO-2. The second difference is that the GO-1 is prepared directly from the synthetic graphite. In contrast, the second type of graphene oxide (GO-2) is prepared from the exfoliated synthetic graphite (elemental analysis C 99.40 %, H 0.01 %) prepared using a high-intensity ultrasound in a pressurized stainless-steel batch reactor [30]. Due to the formation of the exfoliated graphite in the first step of GO-2 production, the subsequent oxidation can be done under much milder conditions using smaller amounts of oxidation agents (60 mL H_2SO_4, 10 mL H_3PO_4, and 3 g $KMnO_4$) [31] compared to GO-1.

2.2.2. Carboxylated graphene oxide (GO-COOH)

The carboxylated graphene oxide (GO-COOH) was prepared according to the literature [32,33] using the water suspension of GO-2 (45 mL; 8 mg/mL) dispersed in water (150 mL) and chloroacetic acid (0.55 g). The reaction mixture was refluxed (6 h), and the product (GO-COOH) was purified by dialysis membrane (Spectra/Por 3).

2.3. Preparation of graphene-based membranes

The membranes were prepared by slow-vacuum filtration of a water suspension of the graphene-derived precursors (GO-1, GO-2 or GO-COOH) on a Pragopor 8 filter (a pore size of 0.23 μm) using a vacuum membrane pump with 20 mbar (abs.) limited pressure. The graphene-based membranes were prepared using different volumes of water suspensions due to various concentrations of graphene-derived precursors. The membranes were typically prepared using 9 mL of GO suspension. However, to get a similar final thickness or to obtain a mechanically robust membrane, it was necessary to vary from 3 to 12 mL (see Table 1). The thickness of dried membranes

was measured with a micrometre at ten locations on the membrane and then averaged.

2.4. Methods of characterization

The graphene-derived precursors (GO-1, GO-2 and GO-COOH) were characterized by X-ray powder diffraction (XRD), infrared spectroscopy (FTIR), Raman spectroscopies, elemental analysis and atomic force microscopic (AFM). All graphene-based membranes were further characterized by XPS, scanning electron microscopy (SEM) and FTIR to compare any changes caused by the preparation process.

XRD was collected on Bruker D2 diffractometer with conventional X-ray tube (CuKα radiation, 30 kV, 10 mA), primary divergence slit module width 0.6 mm, Airscatter screen module 2 mm, Soler Module 2.5, Ni Kbeta-filter 0.5 mm, range 5–90°, step 0.00809°, time per step 1s and the LYNXEYE 1-dimensional detector. A highly diluted water suspension of graphene-derived precursors was dropped on a silicon wafer to form a thin film of the precursor sample. The same Si wafer and holder were always used to minimize experimental error.

The FTIR spectra were recorded on Nicolet Impact 400D spectrometer in the region of 4000-400 cm^{-1} with a resolution of 4 cm^{-1}. The water suspensions were dropped on Si FZ 25.4 mm Ø x 1 mm polished window, and their transmission FTIR spectra were measured. The graphene-based membranes were measured on the same FTIR spectrometer with the diamond ATR crystal.

The Raman spectra were acquired on a DXR Raman microscope (Thermo Scientific) with a 32-two-second scan, laser 532 nm (3 mW) under a 10 × objective of an Olympus microscope.

The Thermo Scientific FlashSmart™ 2000 Elemental analyzer was used for the elemental analysis of the samples. The combustion tube packing was supplied with the instrument and consisted of an EA-2000 chromium oxidizer, high-quality copper reducer and silver cobaltous-cobaltic oxide. Samples (around 1 mg) were weighed in tin containers together with vanadium pentoxide (10 g). All determinations were done in duplicate.

The AFM images were recorded on a Dimension Icon AFM Bruker. The samples were measured with a silicon tip on a nitride lever using ScanAsyst-air contact mode. The mica support was rotated with a drop of sample suspension.

XPS spectra of membranes were obtained on a K-Alpha$^+$ XPS spectrometer (ThermoFisher Scientific, UK), which operated at a base pressure of 1.0×10^{-7} Pa. The Thermo Advantage software (Version 5.9922) was used for data processing and acquisition. Micro-focused (400 μm spot size), monochromatic Al Kα X-rays with a pass energy of 200 eV for the survey and 50 eV for high-energy-resolved core-level spectra were used. The X-ray incidence angle was 30° and the emission angle was along the surface normal. The high-resolution spectra were fitted with Voigt profiles to determine the individual contributions of present chemical species.

The SEM images were done on the FEI Nova NanoSEM450 microscope in a Low-Vacuum mode using an acceleration voltage of 10–20 kV. The graphene-based membranes were cast in EpoThin 2 hardener and EpoThin 2 resin, ground and polished on Vector Power Head (Buehler) and Grinder-Polisher.

2.5. Gas permeability

The time-lag permeation method determined gas permeability through membranes [34]. A high vacuum laboratory apparatus with a static permeation cell was used for measurement samples with an effective membrane area of 1.24 cm^2 at 30 °C. To degas the sample before measurement, the membrane was placed and sealed in a membrane cell and evacuated in the apparatus at 30 °C for 24h. The feed pressure p_i was 1.5 bar. The permeability coefficient P was determined from the increase of permeate pressure Δp_p per time Δt in a calibrated volume V_p of the product part of the membrane cell during a steady state of permeation and calculated using the following equation (Eq. 1):

$$P = \frac{\Delta p_p}{\Delta t} \cdot \frac{V_p . l}{A . p_i} \cdot \frac{1}{RT} \qquad \text{(Eq. 1)}$$

where l is the membrane thickness, A the area, T the temperature, and R the gas constant. Permeabilities are given in units of Barrer (1 Barrer = 1×10^{-10} cm^3(STP) cm/(cm^2 s cm Hg) = 3.35×10^{-16} mol m^{-1} s^{-1}.Pa^{-1}).

The precision of the measurement is better than 3.1 %, as it can be derived from Eq. (1). Relative standard deviation (RSD) of Δp_p and Δt is smaller than 0.3 % (the MKS Barratron pressure transducer precision), RSD of membrane thickness measurement is 1 %, RSD of calibrated volume is less than 0.5 %, and RSD of feed pressure is 0.3 %. For limit cases and P values lower than 0.01 Barrer, the

Table 1
The parameters for graphene-based membrane preparation and membrane thickness.

Sample	Volume of suspension [mL]	Weight [g]	Membrane thickness [μm]
GO-1 (26 μm)	9	0.0981	26
GO-2 (23 μm)	3	0.0609	23[a]
GO-2 (43 μm)	6	0.1218	43
GO-2 (55 μm)	9	0.1827	55
GO-COOH (12 μm)	9	0.0315	12
GO-COOH (25 μm)	12	0.0420	25

[a] Membrane was not mechanically enough robust to enable gas permeation measurements.

measurement error can go up to 10 % and for values < 0.005 Barrer, up to 30 %, respectively.

The following gases were studied in our experiments: H_2, O_2, N_2 and CO_2. Each gas possessed a purity of 99.99 % and was used as received from Messer Technogas s.r.o. (Czech Republic).

From the time-lag data (θ), gas diffusivities (D) were estimated (Eq. (2)):

$$D = \frac{l^2}{6\theta} \quad \text{(Eq. 2)}$$

where l is thickness of the sample. RSD of diffusion coefficients was 4 %.

Apparent solubility coefficients (S) were calculated using the relation (Eq. (3)):

$$S = P/D \quad \text{(Eq. 3)}$$

The overall ideal selectivity (α_{ij}) of a membrane for a pair of gases i and j was expressed by the following equation (Eq. 4):

$$\alpha_{ij} = \frac{P_i}{P_j} = \frac{S_i}{S_j} \cdot \frac{D_i}{D_j} \quad \text{(Eq. 4)}$$

where P_i and P_j are pure gas permeabilities, D_i/D_j is the diffusion selectivity, and S_i/S_j is the solubility selectivity.

3. Results and discussion

3.1. Characterization of graphene-derived precursors

XRD was employed to evaluate the quality of the produced graphene-derived precursors. The position of the diffraction line (001) can predicate the intercalation of resulting cations or the influence of different amounts and arrangement of functional groups on interplanar distance. The XRD patterns (Fig. 1a) show the respective diffraction line (001) at 11.1° (0.80 nm) for GO-1, at 11.2° (0.79 nm) for GO-2, and 11.7° (0.76 nm) for GO-COOH. The significant shift of (001) diffraction line GO-1 < GO-2 < GO-COOH means a slight decrease in interplanar distance due to different content and arrangement of functional groups. According to the literature [35, 36], GO-COOH contains COOH groups arranged on the edges of GO sheets with a negligible amount of C–*O*–C or OH groups on the surface of GO sheets which causes a reduction of interlayer distance.

The FTIR spectra of all graphene-derived precursors (Fig. 1b) contain a very intensive wide band of O–H vibrations at 3000 - 3500 cm^{-1}, the C═O stretching symmetric vibration at 1735 cm^{-1} and C═C skeletal vibration, which overlapping together with O–H vibration and therefore the band is very wide at 1627 cm^{-1} (the most visible for GO-COOH). The presence of epoxy and alkoxy groups is evident from the low intense and wide bands at 1234 and 1049 cm^{-1} (1072 cm^{-1} for GO-COOH). The FTIR spectra show differences in the relative intensity of C═O and C═C, where GO-COOH seems to have a smaller amount of COOH groups. Anyway, due to the presence of the OH band also in the region ~1627 cm^{-1}, it is impossible to draw an unambiguous conclusion about the relative ratio of C═O/C═C band intensities, and the differences among them are negligible.

Raman spectra of GO-1, GO-2 and GO-COOH are shown in Fig. S1. The bands D and G correspond to the breathing mode of C-sp^2 atoms in the ring at 1349 cm^{-1} and the in-plane bond stretching motion of C-sp^2 atoms at 1596 cm^{-1}. No significant change was observed for GO-COOH.

According to elemental analysis (EA) of the bulk materials, GO-1 contained C 44.8 %, H 2.2. %, N 0.3 % and O 52.7 %, while GO-2 showed slightly higher content of C 46.2 %, H 2.5 %, N 1.2 % but lower content of O 50.1 %. Elemental analysis of GO-COOH showed the highest content of C 48.3 %, a similar amount of H 2.5 % and N 1.1 % but the lowest content of O 48.2 %. The smaller content of oxygen and the expected increased content of carbon support the assumption that GO-COOH contains a different number of functional groups than GO-1 and GO-2.

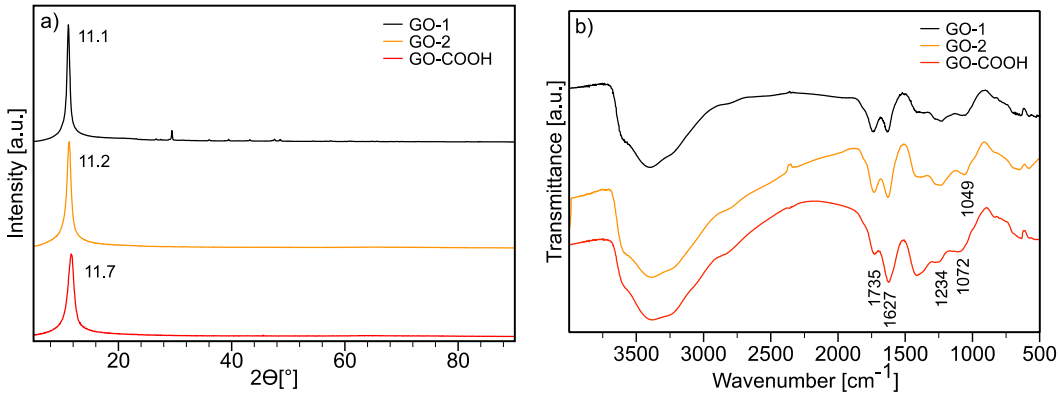

Fig. 1. The graphene-based GO-1, GO-2 and GO-COOH precursors: a) XRD patterns and b) FTIR spectra.

The AFM images showed GO sheets' lateral dimension and height profile with lateral dimensions (~0.8 × 1.2 μm) and a height of ±1 nm corresponding to 2–3 layers of GO. The height profile of the GO-1 and GO-2 sheets are comparable with GO-COOH sheets (Fig. S2), and it was not dependent on the preparation process.

3.2. Characterization of graphene-based membrane

All details of prepared membranes, including membrane thickness, are given in Table 1. First, the thickness of graphene-based membranes was optimized to prepare the thinnest possible self-standing membrane. The GO-1 precursor allowed us to synthesise a 26 μm-thick self-standing membrane, while in the case of the GO-2 precursor, the membrane with a similar thickness (23 μm) was very brittle and broke during the permeation measurements. In contrast, the GO-COOH membrane was successfully prepared with approximately the same thickness (25 μm) as the GO-1 membrane (26 μm). These differences in mechanical robustness of the obtained membranes result from various membrane morphology (well-ordered layered structure of GO-1 and GO-COOH membranes in contrast to cavity-containing disordered structure of GO-2 membrane) as indicated by the SEM images (Fig. 2).

The GO-1 (26 μm) membrane prepared from GO-1 suspension (0.0109 g/mL) seems to be regularly arranged as a layered membrane with longitudinal pores. In contrast, the GO-2 (43 μm) membrane was composed of GO sheets. The GO-2 (55 μm) membrane was prepared from the same starting materials (GO-2 suspension; 0.0203 g/mL), but the filtered amount increased from 0.1218 g to 0.1827 g. The higher amount of filtered solid phase for GO-2 (55 μm) membrane than in the case of GO-2 (43 μm) and the influence of different concentrations of the solid part of GO-2 suspension (0.0203 g/mL) than GO-1 suspension (0.0109 g/mL) could be the reason for faster sedimentation and creation of very compact membrane (Fig. 2). Anyway, a layer of disordered GO sheets was also formed on the membrane surface of GO-2 (55 μm), similar to the case of GO-2 (43 μm) membrane. The GO-COOH membranes (12 and 25 μm) are the most compact, with long longitudinal pores, similar to those in the GO-1 (26 μm) membrane (see Fig. 2). A higher rate of filtration (due to the use of more dilute GO dispersions) evidently promoted the formation of more compact membranes. The reason for various membrane morphologies is probably connected to a slightly different polarity (different content and composition of the oxygen-containing groups) of individual graphene-based precursors, which influences the interactions and stability of GO suspensions [37]. The more polar GO-1 and GO-COOH precursors comprising the higher amounts of oxygen-containing and carboxyl groups, respectively (see above the results of elemental and XPS analysis), led to a formation of the compact membranes with layered GO sheets, probably due to an intense hydrogen bonding. The COOH groups appeared to promote the most intense hydrogen bonding, resulting in the formation of the most compact GO-COOH membrane. In contrast, the less polar GO-2 precursor with low inter-sheet hydrogen bonding produced membranes with fully or partially disordered GO sheets.

The FTIR spectra of all three membranes contained similar characteristic bands as their relevant graphene-derived precursors (see Fig. 1b), showing significantly lower intensities of OH groups in region 3000 - 3500 cm^{-1}. Contrary to the graphene-derived precursors, the FTIR spectra of all prepared graphene-based membranes show the presence of asymmetric stretching C═O band (at 1816 cm^{-1}, Fig. 3). This band is generally less visible in the FTIR spectrum of GO (often only shoulder appeared) [33].

XPS analysis of graphene-based membranes shows us the presence of the same chemical species on the membrane surface, irrespective of the particular modification. The determined chemical composition is presented in Table 2. The C 1s spectra (Fig. S3) of the membranes are mainly dominated by the sp^2 C═C centred at 284.2 eV arising from the aromatic moieties of GO. In addition to it, the C 1s envelope shows contributions of different C–N, ether and alkoxy C–O species (286.4 ± 0.1 eV); ester and carboxyl (C (═O)–O,

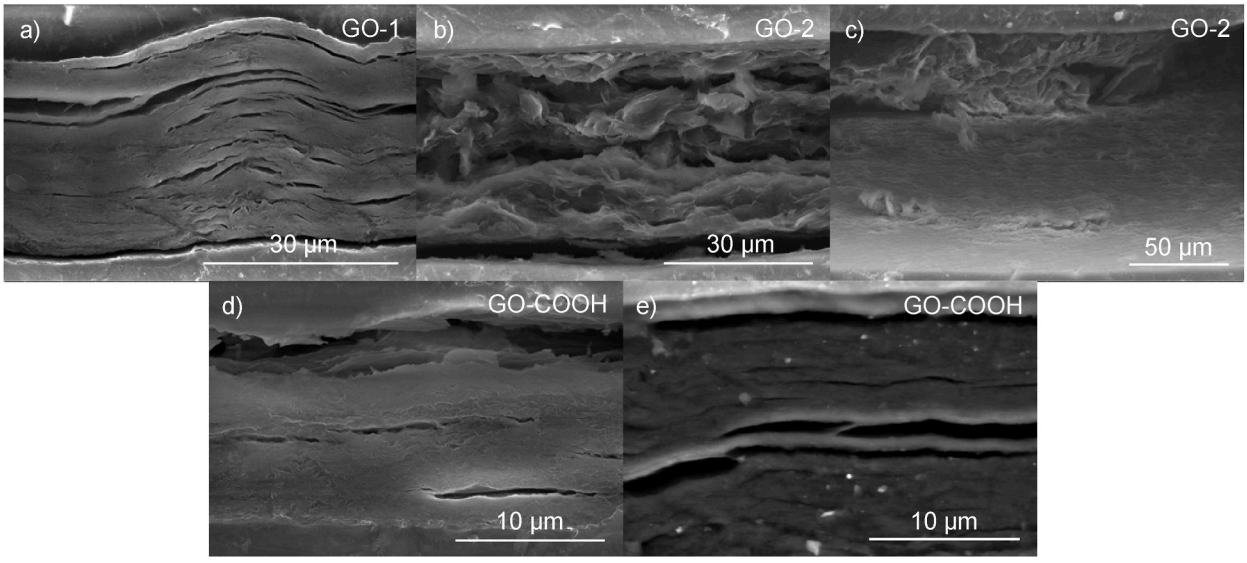

Fig. 2. SEM cross-section images of a) GO-1 (26 μm), b) GO-2 (43 μm), c) GO-2 (55 μm), d) GO-COOH (12 μm), and e) GO-COOH (25 μm) membranes.

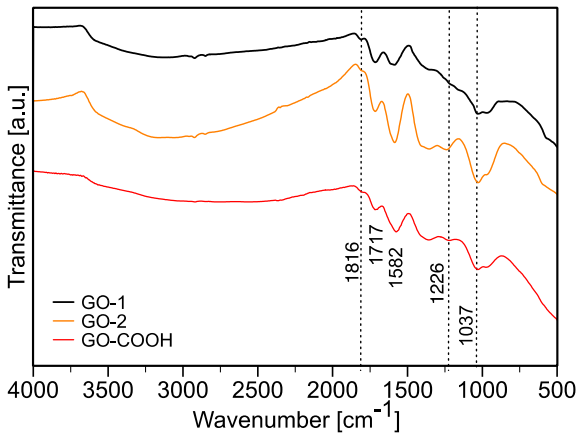

Fig. 3. The FTIR spectra of GO-1, GO-2 and GO-COOH membranes.

Table 2
Surface composition of GO-1, GO-2 and GO-COOH membranes as determined by XPS.

Binding energy [eV]	101.5 ± 0.1	167.2 ± 0.2	284.2	286.4 ± 0.1	288.2 ± 0.2	399.5 ± 0.2	401.2 ± 0.2	532.1 ± 0.2	
	Si 2p SiO_2	S 2p SO_3	C 1s sp^2 C═C	C 1s C–O, C–N	C 1s C═O–O	N 1s NH_2	N 1s N^+H_3	O 1s	COO/sp^2 C‾‾C
Sample	atomic %								
GO-1	3.2 ± 0.3	0.4 ± 0.1	39.7 ± 1.2	21.9 ± 0.6	5.1 ± 0.3	0.6 ± 0.1	0.4 ± 0.1	28.7 ± 0.7	0.1
GO-2	0.2 ± 0.1	0.2 ± 0.1	38.8 ± 2.4	23.4 ± 1.5	7.6 ± 0.7	0.2 ± 0.1	0.4 ± 0.1	29.1 ± 1.1	0.2
GO-COOH	0.1 ± 0.1	0.2 ± 0.1	40.3 ± 0.8	22.8 ± 0.4	7.6 ± 0.2	0.3 ± 0.1	0.4 ± 0.1	28.2 ± 0.6	0.2

(288.2 ± 0.2 eV)) moieties, respectively. The contribution at 290.7 ± 0.2 eV is assigned to the π→π* transition (shakeup) of the aromatic rings. Interestingly, the determined ratio between the C (=O)–O and sp^2 C]C moieties changes from 0.1 for the GO-1 membranes to 0.2 for the GO-2 and GO-COOH membranes. This observation appears to be inconsistent with the findings of FTIR spectroscopy (Figs. 1 and 3). However, it should be considered that FTIR spectroscopy is sensitive to the bulk properties of the analysed material, while the XPS reflects the composition of the surface layer (7–10 nm) of the analysed material. This corresponds to the fact that the C (=O)–O moieties are mainly located on the surface of graphene-based membranes.

3.3. Gas sorption, diffusion, and permeation

The mass of graphene-derived precursor used for membrane preparation is not the only factor affecting membrane thickness, which is also affected by the functionalization of GO sheets (spherical reason, hydrogen interaction, π-π interaction etc.). The structure and thickness of the top layer of the graphene-based membrane also depend upon the rate of membrane formation. Furthermore, it is known that the membrane's selectivity is influenced by the top two or three molecular layers constituting the dense layer of the membrane. At the same time, the remaining substructure affects the overall permeation behaviour [38]. The permeation and separation factor of the membranes is thus affected by interactions of permeate (gas or water vapor) and membrane [39].

The GO-1 (26 μm) membrane exhibited significantly lower permeabilities than the GO-2 (43 μm) and the GO-2 (55 μm) membranes, but the values were still significantly higher than those of GO-COOH membranes (Table 3). The different composition of functional groups of the membranes (the GO-COOH membrane is significantly different from GO-1 and GO-2 membranes) can influence permeabilities. On the other hand, the GO-1 (26 μm) membrane exhibited a more than doubled value for water vapor than all

Table 3
Gas permeability coefficients of graphene-based membranes.

Sample	Membrane thickness (μm)	Permeability coefficients (Barrer)[1]					Ideal selectivity			
		H_2	O_2	N_2	CO_2	H_2O	H_2/CO_2	H_2/N_2	O_2/N_2	CO_2/N_2
GO-1 (26 μm)	26	1.434	0.069	0.006	0.112	33383	12.8	238	11.5	18.6
GO-2 (43 μm)	43	31.063	0.464	0.087	1.224	1601	25.4	357	5.3	14.1
GO-2 (55 μm)	55	9.977	0.495	0.443	1.655	1598	6.0	23	1.1	3.7
GO-COOH (12 μm)	12	0.420	0.002	0.002	0.030	1591	14.2	247	1.3	17.4
GO-COOH (25 μm)	25	0.697	0.010	0.004	0.060	1447	11.6	178	2.6	15.3

other membranes and had the significantly highest O_2/N_2 selectivity of 11.5, which is comparable with the best polymer materials (e.g. poly (substituted acetylenes), Spiro-PIMs (polymer of intrinsic microporosity with spiro-carbons), and polyimides) [40]. The GO-1 (26 μm) membrane contains the highest amount of oxygen and the lowest amount of hydrogen (see above the elemental analysis results); therefore, it is expected to interact via hydrogen bonding with oxygen or water vapor.

Interestingly, we found very high hydrogen permeability and exceptional H_2/CO_2 ideal selectivity for the GO-2 (43 μm) membrane. The selectivity values are several times higher than those of the similar (but thicker) GO-2 (55 μm) membrane. As $P = D.S$, the gas transport of the gas through the material is determined by its diffusion (which occurs in material-free volume) and sorption (gas-material interactions). From the diffusion data in Table 4, we can see that the high hydrogen P value of the GO-2 (43 μm) membrane is dominated by diffusion. Interestingly $P(O_2)$ and $P(N_2)$ are relatively similar to the corresponding values of the GO-2 (55 μm) membrane. This can be explained by the fact that the structure of the GO-2 (43 μm) membrane contains free volume cavities which are accessible only for the small hydrogen molecules (see evidence difference GO-2 (43 μm) from all other membranes on SEM image Fig. 2). This causes a molecular sieving effect providing exceptionally high H_2/CO_2 ideal selectivity. In contrast, the other (larger) molecules do not penetrate the cavities and thus exhibit lower selectivity. H_2/CO_2 separation performance of prepared membranes is compared with the other polymer and composite materials in the Robeson plot [41], which gives in correlation membranes' H_2 permeability vs H_2/CO_2 selectivity (Fig. 4). When is a large set of such data correlated, it can be found certain upper bounds defined by Robeson in 2008 for H_2/CO_2 gas pair, which show limits of polymer membrane separation performance. GO-2 (43 μm) overcomes the Robeson 2008 upper bound and indicates outstanding separation performance, which is comparable in the H_2/CO_2 selectivity with polyaniline [42] and in the $P(H_2)$ values with polyimide [43] membranes.

The membrane gas separation performance strongly depends on the preparation procedure and related graphene sheet sedimentation/orientation. The initial graphene-derived precursor for preparing the GO-2 (55 μm) membrane was the same as those for the GO-2 (43 μm) membrane, but the gas transport properties differed significantly. The reason might be that volume of the suspension of graphene-derived precursors used for membrane preparation via vacuum filtration varied due to different amounts of dry mass in GO-1, GO-2 and GO-COOH suspensions. This might influence the progress of vacuum filtration and modify the rate of sedimentation/membrane formation resulting in different arrangements of GO-sheets in the membrane. It is known that the thickness influence on the gas permeability coefficients is generally negligible in case of >1 μm thick membranes [44] - P is thickness correlated quantity. From the low values of the ideal selectivity of the GO-2 (55 μm) membrane, we can estimate the presence of some voids with the Knudsen flow, which negatively influenced (lowered) the membrane selectivity [45].

Carboxylation of the GO led to the production of membranes with significantly (order of magnitude) decreased permeabilities. From the diffusion data, the GO-COOH sheets packing is much more efficient/denser than the GO membranes (Fig. 2), resulting in a slower rate of gas diffusion. The GO-COOH (25 μm) membrane had slightly higher permeabilities and diffusion coefficients than the GO-COOH (12 μm) membrane. In contrast, the GO-COOH (12 μm) membrane had slightly higher selectivity than that of the GO-COOH (25 μm) membrane, except for O_2/N_2 gas pair. This is due to a relatively high error in the measurement, where the permeability values were close to the detection limit of the apparatus.

The sorption data in Table 5 shows that the GO-1 (26 μm) membrane interacts more with gas and vapor molecules, mainly with CO_2 and H_2O molecules. The reason can be a more polar character of this membrane (as confirmed by FTIR and XPS) supporting penetrate molecule-membrane interactions.

4. Conclusion

The graphene-based and self-standing membranes from different graphene-derived precursors (2 types of graphene oxide, GO-1 and GO-2, and 1 type of carboxylated graphene oxide, GO-COOH) with thicknesses in the range of 12–55 μm were successfully prepared by slow-vacuum filtration method. It was shown that GO-1 precursor synthesized under strongly oxidizing conditions of the Hummers' method leads to producing a layer-ordered membrane with longitudinal pores, which is sufficiently mechanically robust already at a thickness of 26 μm. In contrast, the GO-2 precursor synthesized under mild oxidative conditions from exfoliated graphene produces a membrane with disordered graphene-derived sheets containing cavities. Consequently, the membrane produced in this way is more brittle; therefore, it is necessary to prepare it with a minimum thickness of 43 μm. The GO-COOH precursor has the most compact membrane containing long longitudinal pores, which is mechanically robust even at a very small thickness (12 μm).

Permeability of the obtained membranes for H_2, O_2, N_2 and CO_2 decreased in order GO-2 > GO-1 > GO-COOH. The GO-1 (26 μm) membrane exhibited the best performance among the membranes for water vapor and showed the highest O_2/N_2 selectivity of 11.5, which is comparable with the best polymer materials. This behaviour is consistent with the finding that GO-1 is the most polar

Table 4
Gas diffusion coefficients of graphene-based membranes.

Sample	Membrane thickness (μm)	Diffusion coefficients x10^8 (cm^2/s)					Ideal diffusion selectivity			
		H_2	O_2	N_2	CO_2	H_2O	H_2/CO_2	H_2/N_2	O_2/N_2	CO_2/N_2
GO-1 (26 μm)	26	7.821	0.338	–	0.005	4.285	1564	–	–	–
GO-2 (43 μm)	43	66.197	0.340	0.196	0.066	3.775	1001	338	1.7	0.3
GO-2 (55 μm)	55	24.500	0.361	0.309	0.078	3.890	314	79	1.2	0.3
GO-COOH (12 μm)	12	1.000	0.007	0.004	0.002	3.770	592	250	1.9	0.4
GO-COOH (25 μm)	25	3.605	0.010	0.007	0.004	4.681	1030	552	1.6	0.5

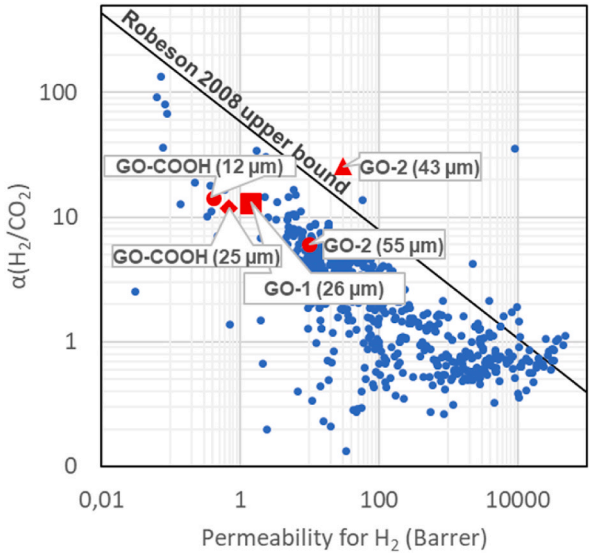

Fig. 4. Permeability for H_2 versus H_2/CO_2 selectivity of graphene-based membranes prepared in this study compared to the most common polymer membranes. The black line indicates the Robeson 2008 upper bound of pure polymer membranes for H_2/CO_2 separation [41].

Table 5
Gas sorption coefficients of graphene-based membranes.

Sample	Membrane thickness (μm)	Solubility coefficients x10^2 (cm^3(STP)/cm^3.cmHg)					Ideal solubility selectivity			
		H_2	O_2	N_2	CO_2	H_2O	H_2/CO_2	H_2/N_2	O_2/N_2	CO_2/N_2
GO-1 (26 μm)	26	0.18	0.21	–	22.40	790	122.2	–	–	–
GO-2 (43 μm)	43	0.47	1.37	0.44	18.51	424	39.5	1.1	3.1	41.7
GO-2 (55 μm)	55	0.41	1.37	1.43	21.22	411	52.1	0.3	1.0	14.8
GO-COOH (12 μm)	12	0.42	0.30	0.43	17.46	422	41.6	1.0	0.7	41.1
GO-COOH (25 μm)	25	0.19	0.97	0.60	17.14	309	88.6	0.3	1.6	28.6

precursor of all three graphene-based precursors because it contains the highest amount of oxygen and the lowest amount of hydrogen. The XPS analysis confirms the predominant presence of C═C groups and the increasing C═C/C═O ratio, especially in the case of GO-2 and GO-COOH membranes. In contrast, the GO-2 (43 μm) membrane showed very high hydrogen permeability while also keeping exceptionally high H_2/CO_2 ideal selectivity, thanks to the arrangement of disordered graphene-derived sheets forming free volume and small-size cavities, which are uniquely accessible for small hydrogen molecules. The GO-2 (43 μm) membrane even overcomes the Robeson 2008 upper bound. The lowest permeability values were observed for the GO-COOH membranes due to too dense packing of graphene-derived sheets in the GO-COOH membrane resulting in a low rate of gas diffusion.

Funding statement

The authors thank the Grant Agency of the Czech Republic (project 22-05244S). This work was also supported by Research Infrastructure NanoEnviCz, supported by the Ministry of Education, Youth and Sports of the Czech Republic under Project No. LM2023066.

Additional information

The authors thank Marie Popovičová for help with graphene oxide preparation, Pavla Kurhajcová for FTIR measurement, Ivo Jakubec for SEM sample preparation of membrane, and Dmytro Bavol for elemental analysis.

Data availability statement

Data generated and utilized for analyses of results presented in this manuscript are available from the corresponding author on request.

CRediT authorship contribution statement

Darina Smržová: Data curation, Formal analysis, Investigation, Methodology, Writing – original draft. **Michaela Šrámová Slušná:** Data curation, Formal analysis, Methodology. **Jakub Peter:** Data curation, Formal analysis, Methodology. **Hynek Beneš:** Conceptualization, Data curation, Project administration, Validation, Writing – original draft, Writing – review & editing. **Jakub Tolasz:** Data curation, Formal analysis, Methodology. **Ognen Pop Georgievski:** Data curation, Formal analysis, Methodology. **Monika Maříková:** Data curation, Formal analysis, Methodology. **Petra Ecorchard:** Conceptualization, Data curation, Formal analysis, Funding acquisition, Project administration, Supervision, Writing – original draft, Writing – review & editing.

Declaration of competing interest

The authors declare that they have no known competing financial interests or personal relationships that could have appeared to influence the work reported in this paper.

Appendix A. Supplementary data

Supplementary data to this article can be found online at https://doi.org/10.1016/j.heliyon.2023.e21417.

References

[1] Z. Wang, C. Ma, C. Xu, S. Sinquefield, M. Shofner, S. Nair, Graphene oxide nanofiltration membranes for desalination under realistic conditions, Nat. Sustain. 4 (5) (2021) 402–408.
[2] P. Kumari, K. Tripathi, L. Jangir, R. Gupta, K. Awasthi, Recent advances in the application of the graphene-based membrane for water purification, Mater. Today Chem. 22 (2021), 100597.
[3] G. Glenn Lipscomb, R. Giraud, Sustainable Separations, Enc. Sustainable Techn. 3 (2017) 553–563.
[4] D. Bastani, N. Esmaeili, M. Asadollahi, Polymeric mixed matrix membranes containing zeolites as a filler for gas separation applications: a review, J. Ind. Eng. Chem. 19 (2) (2013) 375–393.
[5] Q. Xu, H. Xu, J. Chen, Y. Lv, C. Dong, Graphene and graphene oxide: advanced membranes for gas separation and water purification, Inorg. Chem. Front. 2 (2015) 417–424.
[6] A. Morelos-Gomez, R. Cruz-Silva, H. Muramatsu, J. Ortiz-Medina, T. Araki, T. Fukuyo, S. Tejima, K. Takeuchi, T. Hayashi, M. Terrones, M. Endo, Effective NaCl and dye rejection of hybrid graphene oxide/graphene layered membranes, Nat. Nanotechnol. 12 (11) (2017) 1083–1088.
[7] F. Rashidi, N. Kevlich, S. Sinquefield, M.L. Shofner, S. Nair, Graphene oxide membranes in extreme operating environments: concentration of kraft black liquor by lignin retention, ACS Sustain. Chem. Eng. 5 (2017) 1002–1009.
[8] Z. Wang, C. Ma, S.A. Sinquefield, M.L. Shofner, S. Nair, High-performance graphene oxide nanofiltration membranes for black liquor concentration, ACS Sustain. Chem. Eng. 7 (2019) 14915–14923.
[9] Q. Yang, Y. Su, C. Chi, C.T. Cherian, K. Huang, V.G. Kravets, F.C. Wang, J.C. Zhang, A. Pratt, A.N. Grigorenko, F. Guinea, A.K. Geim, R.R. Nair, Ultrathin graphene-based membrane with precise molecular sieving and ultrafast solvent permeation, Nat. Mater. 16 (2017) 1198–1202.
[10] R.K. Joshi, P. Carbone, F.C. Wang, V.G. Kravets, Y. Su, I.V. Grigorieva, H.A. Wu, A.K. Geim, R.R. Nair, Precise and ultrafast molecular sieving through graphene oxide membranes, Science 343 (6172) (2014) 752–754.
[11] J. Abraham, K.S. Vasu, C.D. Williams, K. Gopinadhan, Y. Su, C.T. Cherian, J. Dix, E. Prestat, S.J. Haigh, I.V. Grigorieva, P. Carbone, A.K. Geim, R.R. Nair, Tunable sieving of ions using graphene oxide membranes, Nat. Nanotechnol. 12 (6) (2017) 546–550.
[12] L. Chen, G. Shi, J. Shen, B. Peng, B. Zhang, Y. Wang, F. Bian, J. Wang, D. Li, Z. Qian, G. Xu, G. Liu, J. Zeng, L. Zhang, Y. Yang, et al., Ion sieving in graphene oxide membranes via cationic control of interlayer spacing, Nature 550 (2017) 380–383.
[13] A. Akbari, P. Sheath, S.T. Martin, D.B. Shinde, M. Shaibani, P.C. Banerjee, R. Tkacz, D. Bhattacharyya, M. Majumder, Large-area graphene-based nanofiltration membranes by shear alignment of discotic nematic liquid crystals of graphene oxide, Nat. Commun. 7 (2016), 10891.
[14] D.A. Gkika, V. Karmali, D.A. Lambropoulou, A.C. Mitropoulos, G.Z. Kyzas, Membranes coated with graphene-based materials: a review, Membranes 13 (2) (2023) 1–24, 127.
[15] M.S. Ahmad, Y. Inomata, T. Kida, Energy application of graphene based membrane: hydrogen separation, Chem. Rec. (2023), e202300163.
[16] E.Y.M. Ang, W. Toh, J. Yeo, R. Lin, Z. Liu, K.R. Geethalakshmi, T.Y. Ng, A review on low dimensional carbon desalination and gas separation membrane designs, J. Membr. Sci. 598 (2020), 117785.
[17] P. Liu, J. Hou, Y. Zhang, L. Li, X. Lu, Z. Tang, Two-dimensional material membranes for critical separations, Inorg. Chem. Front. 7 (2020) 2560–2581.
[18] G. Romanos, L.M. Pastrana-Martínez, T. Tsoufis, C. Athanasekou, E. Galata, F. Katsaros, E. Favvas, K.G. Beltsios, E. Siranidi, P. Falaras, V. Psycharis, A.M. T. Silva, J. Membr. Sci. 493 (2015) 734–747.
[19] A. Achari, M. Eswaramoorthy, Casting molecular channels through domain formation: high performance graphene oxide membranes for H_2/CO_2 separation, J. Mater. Chem. A 4 (2016) 7560–7564.
[20] C. Chi, X. Wang, Y. Peng, Y. Qian, Z. Hu, J. Dong, D. Zhao, Facile preparation of graphene oxide membranes for gas separation, Chem. Mater. 28 (9) (2016) 2921–2927.
[21] D. Bouša, K. Friess, K. Pilnáček, O. Vopička, M. Lanč, K. Fónod, M. Pumera, D. Sedmidubský, J. Luxa, Z. Sofer, Thin, high-flux, self-standing, graphene oxide membranes for efficient hydrogen separation from gas mixtures, Chem. Eur J. 23 (2017) 11416–11422.
[22] J. Shen, G. Liu, K. Huang, Z. Chu, W. Jin, N. Xu, Subnanometer two-dimensional graphene oxide channels for ultrafast gas sieving, ACS Nano 10 (3) (2016) 3398–3409.
[23] F. Malekian, H. Ghafourian, K. Zare, A.A. Sharif, Y. Zamani, Recent progress in gas separation using functionalized graphene nanopores and nanoporous graphene oxide membranes, Eur. Phys. J. Plus 134 (212) (2019) 1–12.
[24] Y. Wei, Z. Pastuovic, T. Murphy, D.B. Gore, Precise tuning chemistry and tailoring defects of graphene oxide films by low energy ion beam irradiation Appl, Surf. Sci. 505 (2020), 144651.
[25] L. Huang, W. Jia, H. Lin, Etching and acidifying graphene oxide membranes to increase gas permeance while retaining molecular sieving ability, AIChE J. 66 (e17022) (2020) 1–10.
[26] S. Sharif, K.S. Ahmad, F. Rehman, Z. Bhatti, K.H. Thebo, Two-dimensional graphene oxide based membranes for ionic and molecular separation: current status and challenges, J. Environ. Chem. Eng. 9 (2021), 105605.

[27] C.Y. Chuah, L. Nie, J.-M. Leeb, T.-H. Bae, The influence of cations intercalated in graphene oxide membranes in tuning H_2/CO_2 separation performance, Sep. Purif. Technol. 246 (2020), 116933.
[28] T. Wu, Q. Xue, C. Ling, M. Shan, Z. Liu, Y. Tao, X. Li, Fluorine-modified porous graphene as membrane for CO_2/N_2 separation: molecular dynamic and first-principles simulations, J. Phys. Chem. C 118 (2014) 7369–7376.
[29] D.C. Marcano, D.V. Kosynkin, J.M. Berlin, A. Sinitskii, Z. Sun, A. Slesarev, L.B. Alemany, W. Lu, J.M. Tour, Improved synthesis of graphene oxide, ACS Nano 4 (8) (2010) 4806–4814.
[30] V. Štengl, Preparation of graphene by using an intense cavitation field in a pressurized ultrasonic reactor, Chem. Eur J. 18 (2012) 14047–14054.
[31] V. Štengl, J. Henych, P. Vomáčka, M. Slušná, Doping of TiO_2–GO and TiO_2–rGO with noble metals: synthesis, characterization and photocatalytic performance for azo dye discoloration, Photochem. Photobiol. 89 (2013) 1038–1046.
[32] V. Štengl, S. Bakardjieva, M. Bakardjiev, B. Štíbr, M. Kormunda, Carborane functionalized graphene oxide, a precursor for conductive self-assembled monolayers, Carbon 67 (2014) 336–343.
[33] J. Ederer, P. Janoš, P. Ecorchard, V. Štengl, Z. Bělčická, M. Šťastný, O. Pop-Georgievski, V. Dohnal, Quantitative determination of acidic groups in functionalized graphene by direct titration, React. Funct. Polymers 103 (2016) 44–53.
[34] S.W. Rutherford, D.D. Do, Review of time lag permeation technique as a method for characterisation of porous media and membranes, Adsorption 3 (1997) 283–312.
[35] R.L. White, C.M. White, H. Turgut, A. Massoud, Z.R. Tian, Comparative studies on copper adsorption by graphene oxide and functionalized graphene oxide nanoparticles, J. Taiwan Inst. Chem. Eng. 85 (2018) 18–28.
[36] R. Xing, Y. Li, H. Yu, Preparation of fluoro-functionalized graphene oxide via the Hunsdiecker reaction, Chem. Commun. 52 (2016) 390–393.
[37] K.Z. Donato, H.L. Tan, V.S. Marangoni, M.V.S. Martins, P.R. Ng, M.C.F. Costa, P. Jain, S.J. Lee, G.K.W. Koon, R.K. Donato, A.H.C. Neto, Graphene oxide classification and standardization, Sci. Rep.-UK 13 (2023) 6064.
[38] S. Wang, Z. Tian, S. Dai, D. Jiang, Effect of pore density on gas permeation through nanoporous graphene membranes, Nanoscale 10 (2018) 14660–14666.
[39] P. Pandey, R.S. Chauhan, Preparation of gas separation membranes and their evaluation, Def. Sci. J. 54 (3) (2004) 335–343.
[40] J. Wang, Z. Shi, Y. Zang, H. Jia, M. Teraguchi, T. Kaneko, T. Aoki, Macromolecular design for oxygen/nitrogen permselective membranes—top-performing polymers in 2020, Polymers 13 (17) (2021) 1–39, 3012.
[41] L.M. Robeson, The upper bound revisited, J. Memb. Sci. 320 (1–2) (2008) 390–400.
[42] G. Illing, K. Hellgardt, M. Schonert, R.J. Wakeman, A. Jungbauer, Toward ultrathin polyaniline films for gas separation, J. Memr. Sci. 253 (1–2) (2005) 199–208.
[43] M.E. Rezac, B. Schöberl, Transport and thermal properties of poly(ether imide)/acetylene-terminated monomer blends, J. Memr. Sci. 156 (2) (1999) 211–222.
[44] G. Liu, W. Jin, N. Xu, Graphene-based membranes, Chem. Soc. Rev. 44 (2015) 5016–5030.
[45] P.A. Claisse, Transport Properties of Concrete: Modelling the Durability of Structures, 2020.